Discrete Element Modelling of the packing of spheres and its application to the structure of porous metals made by infiltration of packed beds of NaCl beads

P. Langston and A. R. Kennedy[#]

Faculty of Engineering, University of Nottingham, Nottingham, UK

Email: andrew.kennedy@nottingham.ac.uk; paul.langston@nottingham.ac.uk

[#] Corresponding author: Tel +44 115 9513744

Abstract

A numerical model, using the discrete element method, has been developed to quantify specific parameters that are pertinent to the packing behaviour of relatively large, spherical NaCl beads and mixtures of beads of different sizes. These parameters have been compared with porosity and connectivity measurements made on porous aluminium castings made by molten metal infiltration into packed beds of such beads, after removal of the NaCl by dissolution.

DEM has been found to accurately predict the packing fraction for salt beads with both monosized and binary size distributions and from this the pore fractions in castings made by infiltration into packed beds of beads could be predicted. Through simple development of the condition for contacting of neighbouring beads, the number of windows linking neighbouring pores, and their size, could also be predicted across a wide range of small bead additions. The model also enables an insight into the mixing quality and changes in connectivity introduced through the addition of small beads. This work presents significant progress towards the delivery of a

simulation-based approach to designing preform architectures in order to tailor the resulting porous structures to best suit specific applications.

Keywords

Discrete element method; particle packing; coordination number; porous metals;

1.0 Introduction

Porous metals exhibit important characteristics which enable them to perform well in heat transfer applications. The high thermal conductivity of solid ligaments, the large surface area to volume ratios and their tortuous flow paths, which generate turbulence and high level- mixing in the cooling fluid, offer the potential for devices made from porous metals (for example high power electronic devices [1,2], heat shields, regenerators for thermal engines and thermal energy storage devices incorporating phase change materials [3]) to be compact, efficient and light weight.

Experimental measurement and modelling [4-7] have shown that the thermal characteristics of porous metals are a complex interplay between porosity fraction, pore size, surface area and ligament thickness, as this influences both the thermal properties of the porous metal and its permeability with respect to the fluid flowing through it. Whilst some observations appear to be conflicting, there is general agreement that porous metals with higher relative density and small pore sizes have higher thermal conductivities, while foams which are more “open” are likely to perform better in convective heat transfer due to enhanced thermal dispersion or mixing associated with their higher permeability.

The infiltration of liquid metal into a bed of sacrificial particles (often termed porogens or space fillers) offers a convenient and reproducible method for the manufacture of porous metals [8-11]. Using this method a “preform” is made from the porogen either from loose or tapped beads, or using subsequent

compaction and/or sintering steps. For commercial production, loose packing of the porogen is often sufficient to achieve the target densities and has the advantage that it increases production rates and reduces cost. Infiltration with a molten metal (the process usually pairs metals with space holders that have a higher melting point, for example aluminium and NaCl) is affected by either applying a positive pressure to the metal or a vacuum to the porogen bed. The pore structure in the porous metal is thus a negative of the morphology and spatial arrangement of the porogen, with the potential to differ slightly depending upon the extent of infiltration into the spaces between the beads, which is a function of the infiltration pressure difference used. Important structural features include the size of the pores (dictated by the size of the porogen) the fraction of pores (dictated by their packing behaviour) and the number and size of the windows connecting the pores (dictated by the coordination number for the beads). The benefit of this process is that it has the potential to vary the porosity, ligament thickness and pore size independently.

An ability to model the packing behaviour of porogens will aid in the design of appropriate porous structures to balance the requirements of heat transport characteristics against the pressure drop across the porous structure. Beyond the consideration of simple monosized particle systems, the introduction of different sizes or shapes of beads has the potential to enhance the packing behaviour and to produce novel structures with multi-modal pore sizes and gradient pore structures. Robust modelling is integral to structural optimisation from the wide possibilities of structures that could be produced.

The discrete element method (DEM) is well established as an accurate tool, in a wide range of engineering disciplines, for modelling of packing and flow in granular materials [12-13]. Whilst DEM has been used to model the packing of monosized particle and binary mixtures and compare the predictions with experimental measurements [14-17] and has been applied to the packing of monosized NaCl particles that formed the basis for a preform to make porous Al [18], previous studies have not combined these elements and applied them to full-scale modelling of porogen packing and then compared

the modelling predictions to structural parameters measured from porous metals made by infiltration of these packed structures.

2.0 Materials and methods: Preparation of porous samples

In order to vary the density and interconnectivity of porous structures, two different spherical salt bead (porogen) sizes were used, achieved by sieving:

- the larger (L) with a size range between 2.0 and 2.5 mm and
- the smaller (S) between 0.5 and 1.0 mm.

In both cases the beads have a density, measured by mercury intrusion porosimetry, between 1.65 and 1.68 g/cc. Details of the materials and methods used to make the beads are given in [10,11,19]. Castings were made by pouring salt beads (with different volumetric fractions of large and small beads, mixed using a turbula mixer) into a 35mm diameter flanged stainless steel mould with a porous base. The flanged mould was pre-heated to 600°C and part-inserted into a vacuum chamber and when molten 99.5% Al (at 800°C) was poured onto the top of the bed of beads, a 0.9 bar pressure differential was applied to drive infiltration of the molten metal therein. Cast samples were machined into 33 mm diameter cylinders, 40 mm long, whereafter the salt beads were removed by dissolution in warm water. Images of the 2.-2.5mm spherical beads and the vacuum infiltration vessel containing the mould are presented in Fig 1.

3. 0 Simulation procedure: Packing modelling using DEM and experimental verification

The packing behaviour was simulated using DEM. The DEM technique applied here uses an explicit time stepping approach to numerically integrate the motion of each particle from the resulting forces acting on them at each timestep. The model follows a fairly standard DEM

approach for spheres. The inter-particle and particle wall contacts are modelled using the spring–dashpot–slider analogy. Contact forces are modelled in the normal and tangential directions with respect to the line connecting the particles centres. Particle cohesion and interstitial fluid effects can also be modelled but were not considered in this study owing to the large particle sizes. Inter-particle and particle-wall friction were considered and the friction coefficients were estimated from the critical angle for the onset of sliding of a "raft" of salt beads down the requisite surfaces (including a surface made from another "raft" of salt beads). Rolling friction is modelled as an angular torque arising from the elastic hysteresis loss or viscous dissipation [20]. The translational and rotational motion of each particle is modelled using a half step leap-frog Verlet numerical integration scheme to update particle positions and velocities. A zoning method and near-neighbour lists are used to increase the computational efficiency of determining particle contacts [21]. A number of techniques can be used to extend the model to include non-spherical particles eg [22] but spherical particles are quite adequate for this case and easier to model.

Fig 2 shows an example of near-mono-sized particles filling a cylindrical vessel (the "mould") under gravity and settling as modelled here. Particles are added gradually in layers. Each particle is given a random initial velocity within a narrow range, similarly the particle size is randomised within a specified range (using a normal distribution). Although the "monosized" system does not comprise of particles with a single diameter, it is subsequently named so to avoid confusion with binary systems. Binary systems were also simulated with random seeding of particle types (differing in size and volume fraction). Table 1 shows the principal data used in the simulations; where the number, size and density match the experiments closely, typical damping properties are also used.

At the end of the simulation, when the particles have settled (essentially the simulation is run until the max particle velocity is very small), the DEM model outputs the type, x, y, z coordinates and radius for every particle. The fill height (and hence the global packing fraction) is determined

from the average z position for particles in the top layer of the vessel. Additionally, the packing fraction within a smaller "sensor" region can be measured to eliminate the effects of poor packing at the walls. The results are analysed in a simple program to produce graphical representations of the packing behaviour (eg Fig 2) and the coordination number can be calculated by computing the distance between each particle and its neighbours.

In order to consider whether particles would become connected pores in the porous metal, the extent of metal infiltration was also considered. This was necessary as two particles in very close proximity, but not actually touching, may end up becoming connected pores if the gap separating them cannot be filled with the infiltrating liquid. The minimum gap that can be filled with the infiltrating liquid was determined from the Laplace equation (shown in equation 1) which relates the applied pressure, P, to the capillary radius, r_c, using established wetting data for the Al-NaCl system [10,11] to determine the liquid surface tension, σ_{LV} and the contact angle, θ. A typical capillary radius for this system and process is of the order of 15 μm and hence particle separations below 30 μm were deemed to be "contacting". The coordination number was calculated for every particle within a smaller "sensor" volume to eliminate "missing" neighbours for particles contacting the walls of the vessel.

$$r_c = \frac{2\sigma_{LV}\cos\theta}{P} \qquad \text{Equation 1}$$

The packing simulation was compared with experimental filling of graduated cylinders of different diameters with salt beads. A funnel was used in order to ensure a repeatable filling action. In order to minimise cohesive effects, the salt particles were thoroughly dried before use. The number of particles used in the simulation was varied in order to keep the fill heights the

same for both the modelled and experimental cases (so in all cases a full scale version of the experiment was modelled) and so that the fill height was larger than the vessel diameter.

The density of porous metal structures was simply measured from the volume and mass. Pore and window structures were investigated using optical and scanning electron microscopy (SEM) combined with image analysis. Micro-computed X-ray tomography (micro CT) on a GE Nanotom system (at a voxel size of 10 μm) was used to examine and quantify the structures of the porous metals. The coordination number for cast porous metal structures was determined from CT images and image analysis using Aviso Fire software. Since the pores in the casting are connected, they were first thresholded and then separated using a watershed algorithm similar to those used in [17,18]. From this, the volume of the object was determined, along with the x, y, z co-ordinates for the centroid and the radius of a sphere with equivalent volume. As the beads were close to spherical in shape and do not undergo distortion during filling and infiltration, it was deemed that this approach should yield acceptable errors. The 3D objects were then sorted, where appropriate, into large and small particles, yielding the same format of analysis input data as for the simulations. Data were processed in the same way as described for the simulation data, with the exception that the separation condition also included the thickness of the sphere that was eroded in order to affect separation. Fig 3 shows snapshots from the Aviso software showing the output after separation. The number of large particles sampled was at least 1000 and exceeded that used in a similar study where the sample size was deemed to be sufficient for reliable statistics [18].

4.0 Results and discussion

4.1 Overview of cast porous metal structures

Fig 4 shows the typical characteristics of porous metals made by replication of packed beds of spherical NaCl beads. The pores clearly retain the size and shape of the original NaCl spheres and approximately circular windows link adjacent pores, the number of which is dictated by the coordination number.

4.2 Comparison of experiment and packing model

The experimental and modelled "global" packing fractions for monosized beads packed into measuring vessels of different sizes are shown in Fig 5. The agreement between the two is good, the modelled values generally falling within the scatter of the experimental values (whilst the repeatability in the results is good, the experimental scatter is fairly high given the imprecision of reading the vertical scale for a non-flat surface of the bed of beads. The sensitivity to the coefficient of friction was tested in the range of 0.2 to 0.4 and was found to affect the packing fraction by less than 0.5% (this compares with a typical scatter in experimental data of 3%).

An effect of vessel size is observed, with an increase in packing fraction from 0.56 to nearly 0.59 as the vessel to bead size ratio increases from 8 (for 18 mm) to nearly 18 (for 40 mm). Poorer packing is expected in narrower vessels due to the increasing contribution of "wall" effects for these relatively "small" systems [23]. The packing fraction is approximately constant for a vessel / bead size ratio greater than 12, a similar effect to that reported in [23-25]. Although not presented, the effect of bed height on the packing fraction was also determined. When the height was again greater than roughly 10 times the bead diameter, there was little effect of further increases in bed height, agreeing well with experimental measurements in [25]. Although not crucial, since the full system is modelled, the mould diameter and fill height used in experiments and modelling for the castings were above the observed limits.

The packing fractions observed and modelled are consistent with previous studies which report the “loose” packing fraction for monosized spheres to be between 0.55 and 0.58, depending upon the friction conditions and the limit of random dense packing for monosized spheres, under frictionless conditions, which is 0.64 [14,16,17,26,27]. The effect of a distribution in particle size (in this case a standard deviation of roughly 10%) for the “monosized” case is unlikely to enhance the packing behaviour, with benefits only thought to be likely for deviations greater than 30% [18,27].

The effect of additions of smaller particles was investigated for the full-sized representation of 35 mm diameter casting moulds. Fig 6 shows the experimental and modelled global packing fraction as a function of small bead solid volume percent, along with a representative vertical section through the modelled packed structure for a 12.5vol.% small particle addition (Note vol.% here implies solid volume %.). The model and the experiments are in good agreement with both cases showing that the addition of small beads increases the packing fraction from roughly 0.58 to a maximum of 0.65 at an addition level close to 25vol.%, decreasing slightly thereafter with increasing additions. Data are near identical when a smaller “sensor” region was used to mimic the exact size of the machined casting (33 mm) as only one large particle diameter is removed from the overall cross section. The packing behaviour is in broad agreement with observations from other researchers [15,23,28] who, for a particle size ratios between 2 and 3, found maximum packing fractions were achieved with between 25 and 30vol.% additions of small particles. Figure 7 shows horizontal sections at the mid-plane for the modelled particle distributions (for 35mm vessels) and for CT images from corresponding samples (33 mm in diameter after the surface is machined) and the simulation can be seen to replicate, quite accurately, the typical features for the packing of these beads (for example regions with locally high packing and others with voids).

Table 2 shows the relationship between the relative density (or metal fraction) for at least 4 cast samples for each porous metal type (after removal of the salt beads), the porosity calculated from packing experiments and the global porosity predicted by the model. In all cases the metal fractions in the cast parts are in good agreement, but consistently slightly lower than those for the fraction of void space determined from the experimental measurements of the packing fraction of the beads and from the model. This discrepancy is most likely to be due to incomplete filling of all the void space in the porous preform under the relatively modest infiltration pressure.

Fig 8 shows the variation in packing fraction as a function of fractional height from the base of the sample for both the monosized beads and with 25vol.% addition of small particles and compares it with 2D area fraction data from CT measurements. The modelled profile is more undulating (with a smaller period). The mean values are 0.58 and 0.65 for both the modelled and experimental data, with lower standard deviations for the monosized bead structures (1.6 and 2.8% of the mean for modelled and experimental data respectively) compared with 1.8 and 3.6% for structures with 25vol.% of small bead additions. This reflects what is observed, that in reality, packing and mixing of the large and small beads is less homogeneous than is predicted by the model. Modelling and experimental data (summarised in Table 3) indicate that the standard deviation in the packing fraction decreases with increasing additions of small particles showing, as was apparent from the images in Fig 7 that more homogenous structures are produced with higher proportion of small particles.

Fig 9 shows SEM images and 2D sections from 3D CT reconstructions for the monosized sample and for a bimodal structure with 25vol.% addition of small particles. It is clear that the number of windows joining the pores (dictated by the coordination number) increases significantly when small particles are introduced into the system. When inspecting the internal surface of the large pores it is not obvious which windows are those linking to small or other large pores.

The coordination number for the modelled samples is compared with the coordination number determined from image analysis of the cast samples. As the segmentation and separation process

was thought to be more likely to create errors in the centroid positions and radii for the small beads, the coordination for large particles (L-L and L-S) were determined and it was assumed that if this could be predicted correctly then the model would be a sufficiently accurate representation of the entire structure and the other contacts (S-S and S-L) would be predicted with the same precision. Fig 10 presents an overview for the L-L and L-S co-ordination numbers for both the model and the experimental data. There is once more, good agreement, with the experimental data and the error bars (±1 standard deviation) lie within the mean value for the model and bands (dashed lines) ±1 standard deviation above and below the mean.

Table 4 presents the mean and standard deviations for the model and those measured experimentally. Modelling and experimentation both indicate packed structures with an average coordination number between 6.3 and 6.5. These values are slightly above those measured and simulated for monosized samples exhibiting loose or dense random packing, between 5 and 6 [14,26]. This difference is attributed to the effect of increasing the "connectivity" via the necessary condition that liquid must infiltrate between separated particles and is not unlike experimental methods to measure connectivity using a liquid bridging technique, which yields higher coordination numbers for monosized particles (6.2, [23]) when compared with other measurement methods or simulations. It is worth noting that if the condition of exactly contacting spheres is used, i.e. $r_c = 0$, the "true" coordination number for monosized spheres is 5.6 ±1.45 which is in good agreement with that expected for loose packing [14,16,23,26,28].

The sensitivity of the coordination number to the capillary radius may be questioned. Although the capillary radius is based on experimental data, there is some uncertainty in these measurements. A radius of 15 μm was used and it is expected that the variation, based on possible variations in pressure and wetting data could be ± 3 μm, resulting in a change in the mean co-ordination number (for monosized spheres) of only ± 0.1. For comparison, the coordination number predicted by DEM has a scatter of ± 1.4. Other possible errors include the

friction coefficient in the model, although it was found that variation in the range of 0.2 to 0.4 altered the coordination number by only 0.2, and the image digitisation and watershed processes are likely to introduce some errors into the experimental measurement of coordination number.

The decrease in N L-L with increasing additions of small particles shows that the small particles, despite their 1:3 size ratio, do not sit in the interstices in the packed structure, even at low additions, where they would do little to disturb the co-ordination of the large particles. Instead, they cause increased disruption of the network of L-L contacts such that for 50vol.% additions the model predicts an average L-L coordination number of 2.1 (±1.12), indicating that a significant number of large particles will have only one large particle as a neighbour, preventing the formation of a completely connected network of large particles. This is a useful insight as such an effect on the connectivity could have a significant influence on the transport properties within the porous structure.

Fig 11 scrutinises the contacts in the binary samples in more detail, distinguishing between each different contact type and calculating the overall coordination number, which of course reflects that there are very many more small beads than large, even at the lower addition levels. As shown previously, N L-L decreases and N L-S increases significantly with small particle additions. The model also predicts that N S-S increases and N S-L decreases with increasing small particle additions (in both cases to a lesser degree than for the large particles given that the capacity for high values of N for small particles is, of course, limited by their size). Despite the very high coordination number for the large particles, their low number fraction means that the average coordination number increases very little with increasing additions (from 6.3 to 7.0 over the full range of addition). This observation is similar to that observed in [23,28]. It is also reported that the maximum number of small particles that might be randomly placed on a large sphere (the so-called parking number [28,29]) can be determined for a particular particle size ratio, for this system it is 35. For 50vol.% additions the L-S coordination number is 26±4.5, below this upper limit.

Fig 12 shows the large increase in the number of windows connecting pores in cast porous metals made with 25vol.% addition of small beads. At these higher magnifications it is apparent that 3-4 pores are visible in a half section of a pore for monosized beads, increasing to more than 10 windows with 25vol.% addition of small particles. For the large particles, the model predicts that for 25vol.% addition of small beads, only 21% (roughly one in 5) of the windows will be connecting to another large particle.

The standard deviation in N L-S can be used as an indication of the quality of mixing. For both the modelled and experimental data, the standard deviation (as a percentage of the mean N L-S coordination number) decreases with increasing addition of small particles and is in agreement with the findings for the effect on the standard deviation in the packing fraction. Both measures, therefore, indicate improved homogeneity of mixing with increasing additions of small particles. As before, the model predicts more homogeneous mixing than is observed in reality, a factor related to the randomised seeding of small particles which will produce a more uniform dispersion than can be achieved through mixing. Although the indications are good, further modelling would be required to establish its efficacy as a tool to predict mixing quality in multi-modal particle systems.

4.3 Window size model

Further simple analysis can be used to predict the size of the windows joining the pores that are a result of contacts between L-L, L-S or S-S beads. Fig 13 presents 2D CT images of porous cast structures (containing 25vol.% particle additions) that have been processed using an edge-finding function to highlight the periphery of the pores. These images clearly show the connections or “windows” between L-L, L-S and S-S contacts. Measurement of the size of these connections from such images is difficult and SEM measurement was preferred, but nevertheless difficult given the non-planar surface and the difficulty distinguishing between the different connection types. For this reason only a small fraction of the windows were measured, restricted to those that were suitably oriented to the viewing angle. L-L connections were simple to measure from samples with no small particle additions and S-S data were

compared with those from a sample made from 100% small beads prepared as part of another study by these authors. Measurements of L-S connections were made by selective choice of what appeared to be representative windows in large pores in samples with high additions of small particles. Whilst for samples with 37.5% additions of small beads, 88% of the connections are L-S, it is possible that the values for the L-S measurements (which are, of course the same as S-L) may be skewed to higher values given the possibility of including some L-L connections in the measurements. Table 4 presents the measured values for the window sizes, showing quite large standard deviations, most likely due to the measurement method, but also reflecting the range in bead sizes. It is apparent that although, as expected, the window between small beads is smaller, the ratio of window to pore size for the small beads (0.28) is much higher than that for the large beads (0.17).

A simple geometric model is presented which is based on the contacting of spheres and the bridging of this connection by a liquid front of a given radius, again defined by the capillarity, as is the condition for assessment of contacting particles in the DEM model. A schematic of this arrangement is shown in Fig 14. Table 5 compares the measured and modelled values for the window sizes. The scatter in the model is due to calculation of the maximum and minimum hole sizes that could occur from contacts between the largest and smallest particles in the size range. Despite the difficulties in accurate measurement, and the less good agreement for the L-S contacts, the measured window sizes are broadly consistent with the model.

5.0 Conclusions

A DEM model has been developed to quantify specific parameters that are pertinent to the packing behaviour of relatively large, near spherical NaCl beads including mixtures of beads of different sizes.

DEM has been found to accurately predict the packing fraction for salt beads with both monosized and binary size distributions and from this the pore fractions in castings made by infiltration into packed beds of beads.

Through simple development of the condition for contacting of neighbouring beads, the number of windows linking neighbouring pores, and their size, could also be predicted for a wide range of small bead additions, enabling insight into the connectivity of the structure.

This work presents significant progress towards the delivery of a simulation-based approach to designing preform architectures in order to tailor the resulting porous structures to best suit specific applications.

The DEM model could be developed further to model non-spherical particles, mould tapping or vibration, particle cohesion and interstitial fluid effects which may be more significant for smaller particles.

References

1. K. Boosma, D Poulikakos, F Zwick, Mechanics of Materials 35 (2003) 1161-1176.
2. T.J. Lu, A. G. Evans, J. W Hutchinson, Trans ASME Journal of Electronic Packaging 12 (1998) 120-130.
3. T. J Lu, H. A Stone, M. F Ashby, Acta Metall 46 (1998) 3619-3635.
4. A.Bhattacharya, V. V. Calmidi, R. N. Mahajan,, International J. Heat Mass Trans, 2002, 45, 1017- 1031.
5. C, Y. Zhao, T. J. Lu, H. P. Hutson, J. D. Jackson, Mater Sci and Eng 367 (2004) 123-131.
6. A. Bhattachyra, R. N. Mahayan, Journal of Electronic Packaging 126 (2006) 259-266.
7. D. Angirasa, J of Heat Trans 124 (2002) 739-745.

8. R. Goodall, J.F. Despois, A. Marmottant, L. Salvo, A. Mortensen, Scripta Mater. 54 (2006) 2069-2073.

9. R. Goodall, A. Marmottant, L. Salvo, A. Mortensen, Mat Sci Eng: A465 (2007) 124-135.

10. A. Jinnapat, A.R. Kennedy, Metals, 1 (2011) 49-64.

11. A. Jinnapat, A.R. Kennedy, Metals, 2 (2012) 122-135.

12. P. A. Cundall, O. D. L. Strack, Géotechnique 29 (1979) 47-65.

13. F. Y. Fraige, P. A. Langston, A. J. Matchett, J. Dodds, Particuology, 6 (2008) 455-466.

14. W. van Antwerpen, C.G. du Toit, P.G. Rousseau, Nuclear Engineering and Design, 240 (2010) 1803–1818.

15. Y. Gan, M. Kamlah, J. Reimann, Fusion Engineering and Design 85 (2010) 1782–1787.

16. J-F. Jerier, V. Richefeu, D. Imbault, F-V. Donzé, Computer Methods in Applied Mechanics and Engineering 199 (2010) 1668–1676.

17. X. Fu, M. A. Dutt, C. Bentham, B. C. Hancock, R. E. Cameron, J. A. Elliott, Powder Technology 167 (2006) 134–140.

18. A. Marmottant, L. Salvo, C.L. Martin, A. Mortensen, Journal of the European Ceramic Society, 28 (2008) 2441-2449.

19. A Jinnapat, A.R. Kennedy, J. Alloys and Compounds, 499 (2010) 43-47.

20. Y. C.Zhou, B. H. Xu, A. B.Yu , P. Zulli, Powder Technology 125 (2002) 45-54.

21. B. N.Asmar, P. A., Langston, A. J. Matchett, J. K. Walters, Computers and Chemical Engineering 26 (2002) 785-802.

22. S.Mack, P. A. Langston, C.Webb, T. York, Powder Technology 214 (2011) 431-442.

23. D. Pinson, R.P Zou, A.B. Yu, P Zulli, M.J. McCarthy, , J Phys D, Appl. Phys. 31 (1998) 457-462.

24. G. E. Mueller, Powder Technology 92 (1997) 179-183.

25. R.P Zou, A.B. Yu, Chemical Engineering Science, 50 (1995) 1504–1507.

26. L. E. Silbert, Soft Matter, 6 (2010) 2918-2924.

27. N. D. Aparicio, A.C.F. Cocks, Acta Metall, 43 (1995) 3873-3884.

28. K. de Lange Kristiansen, A. Wouterse, A. Philipse, Physica A: Statistical Mechanics and its Applications, 358 (2005) 249–262.

29. M.L. Mansfield, L. Rakesh, D.A. Tomalia, J. Chem. Phys., 105 (1996) 3245.

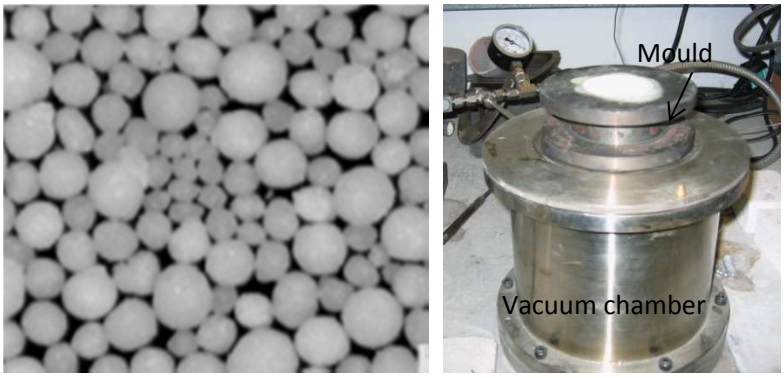

Fig 1. Left, 2.0-2.5 mm salt beads, right, vacuum casting chamber containing the mould

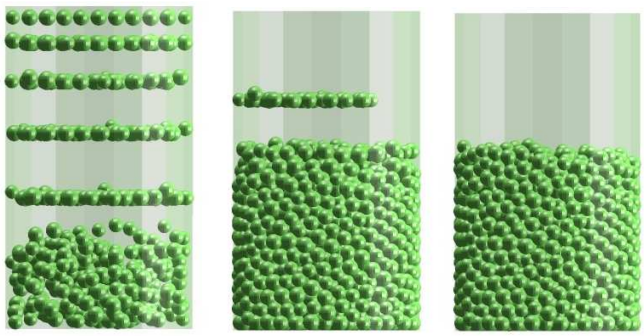

a) b) c)

Fig 2 DEM simulation of the filling of a 35mm diameter vessel with monosized beads (time a) 0.1, b) 0.3 and c) 0.5 s)

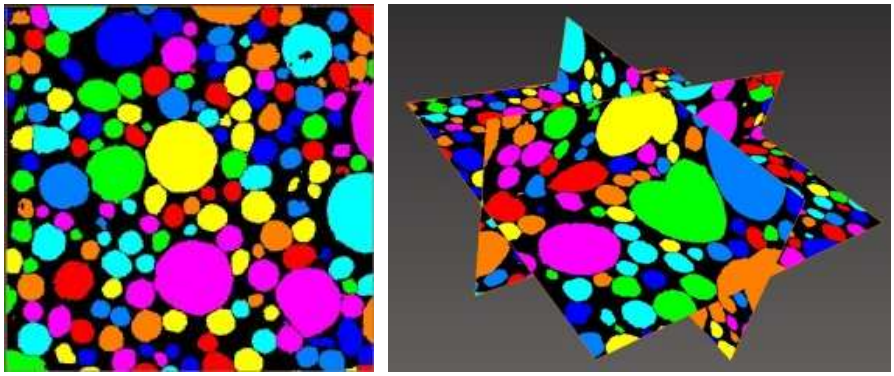

Fig 3 Thresholded and separated pores for bimodal particle distributions containing 25vol.% of small particles

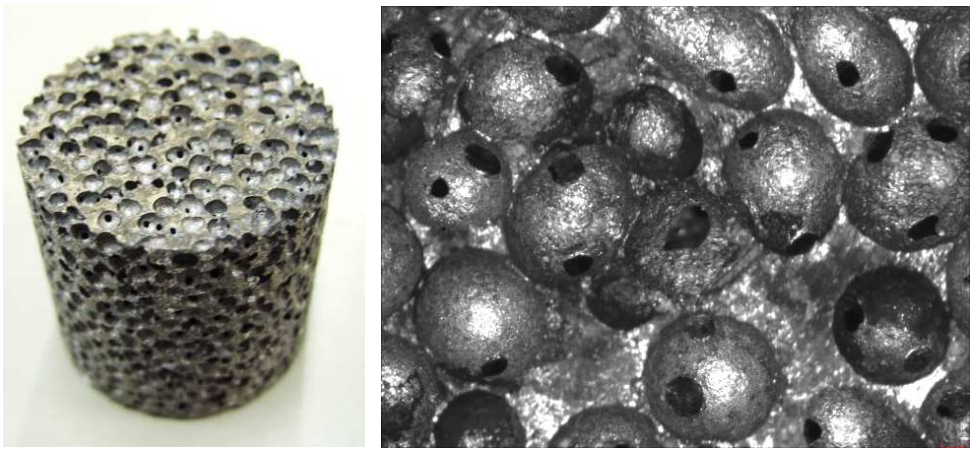

Fig 4 Optical micrographs, left of a porous sample made by vacuum casting using monosized NaCl beads and right, showing the spherical pore structures and windows between pores

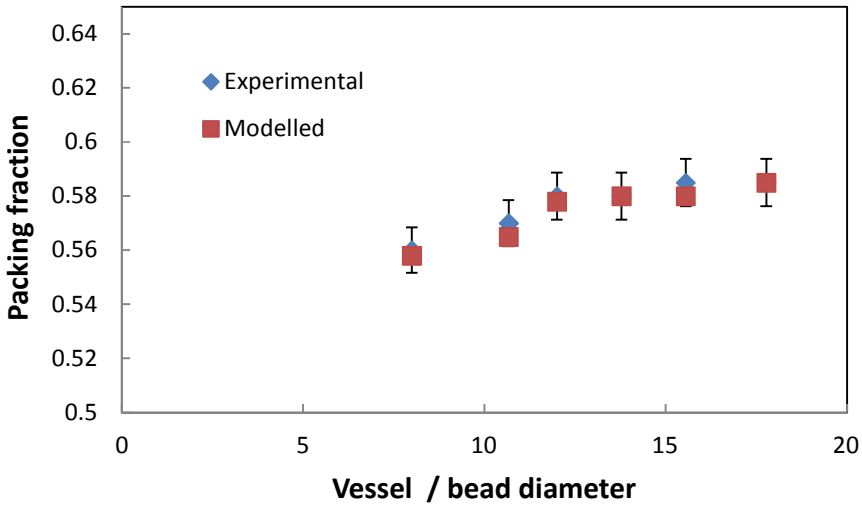

Fig 5 Modelled and experimental packing behaviour for monosized (2.0-2.5 mm) beads in vessels of different diameters

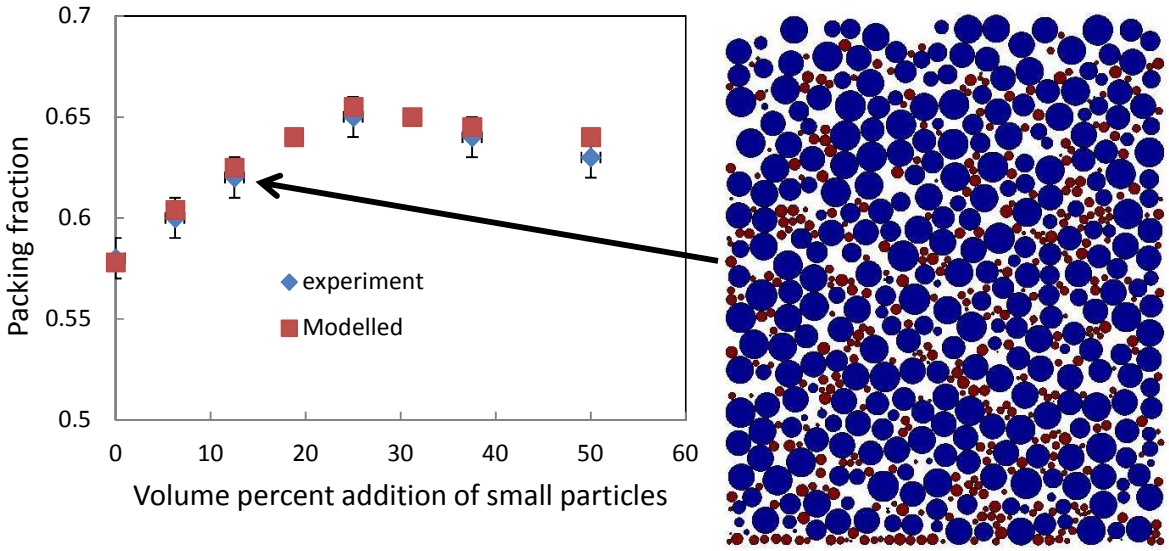

Fig 6 Left**,** experimental and modelled packing fraction as a function of the volume percentage of small beads and right, a vertical section through the modelled packed structure for a 12.5vol.% small particle addition

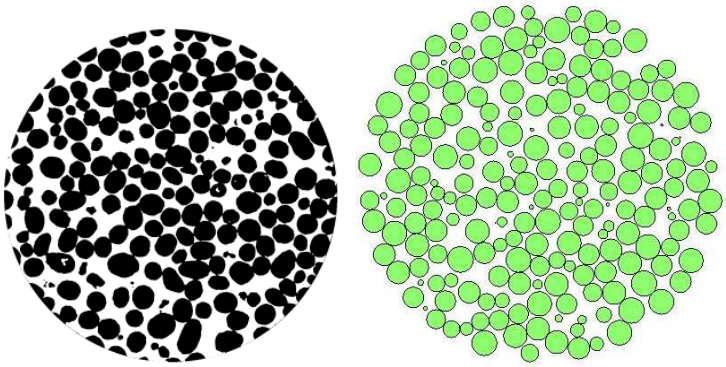

a)

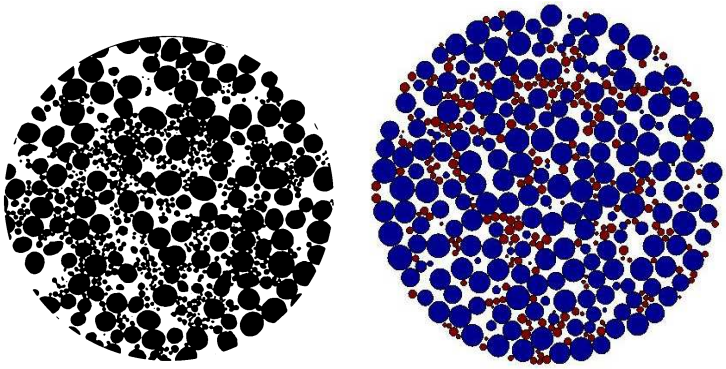

b)

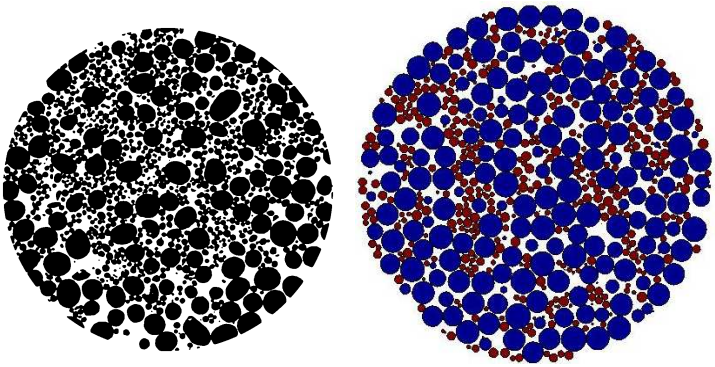

c)

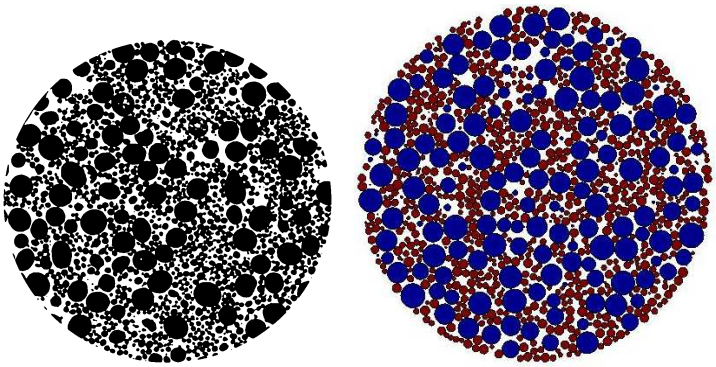

d)

Fig 7 Horizontal sections at the mid-plane for, left, experimental samples (CT images from 33 mm diameter samples after the surface is machined) and right, modelled packed structures (for 35mm vessels) for different additions of small particles, a) 0, b) 12.5, C) 25 and d) 37.5vol.%.

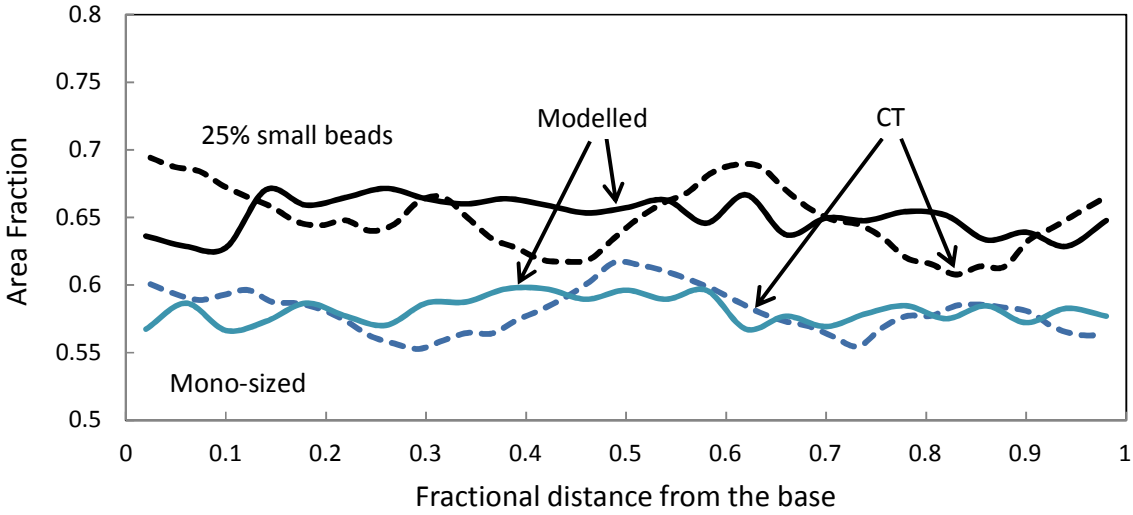

Fig 8 Experimental and modelled profiles for packing as a function of height through the sample for monosized and bimodal mixtures containing 25vol.% small particles

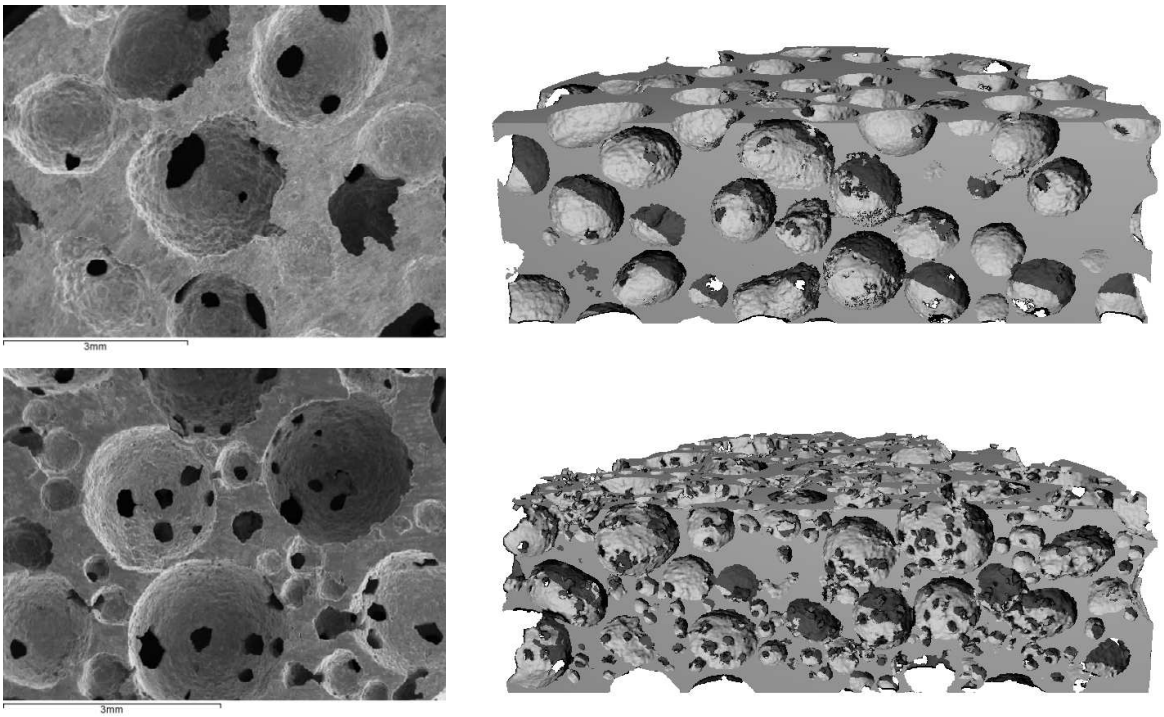

Fig 9 SEM and CT images of cast porous metals for top, monosized beads and bottom, for 25vol.% addition of small beads

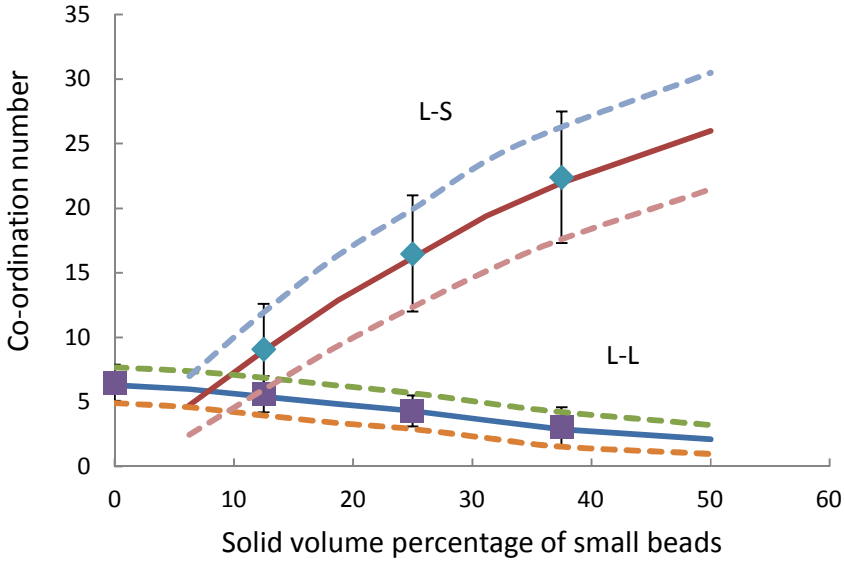

Fig 10 Plots of modelled (solid lines) and experimental (symbols) L-L and L-S co-ordination numbers. Dashed lines and error bars indicate 1 standard deviation in the modelled and experimental data respectively.

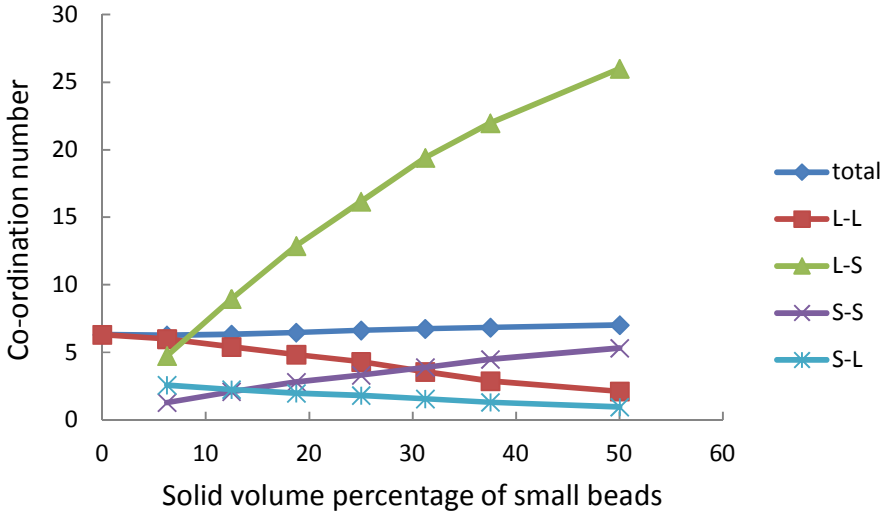

Fig 11 Breakdown of individual (modelled) contact types and total for 25vol.% addition of small particles

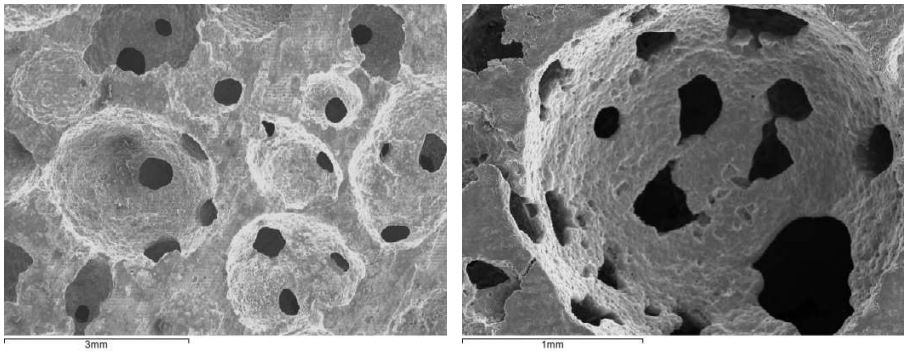

Fig 12 SEM images of pore windows in castings made from, left, monosized beads and right, with 25vol.% additions of small beads

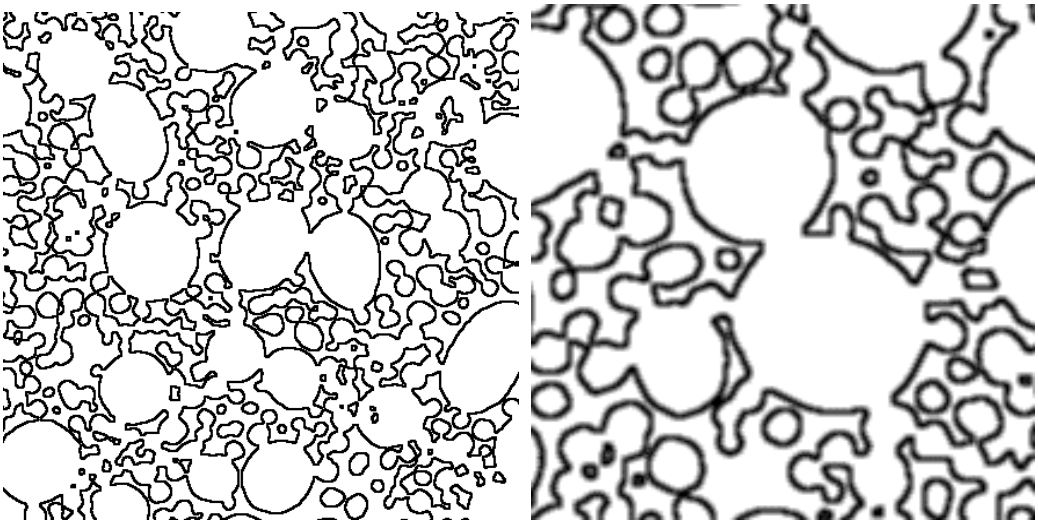

Fig 13 2D CT images of porous metal castings containing 25% of small particles, highlighting the connections and windows between pores

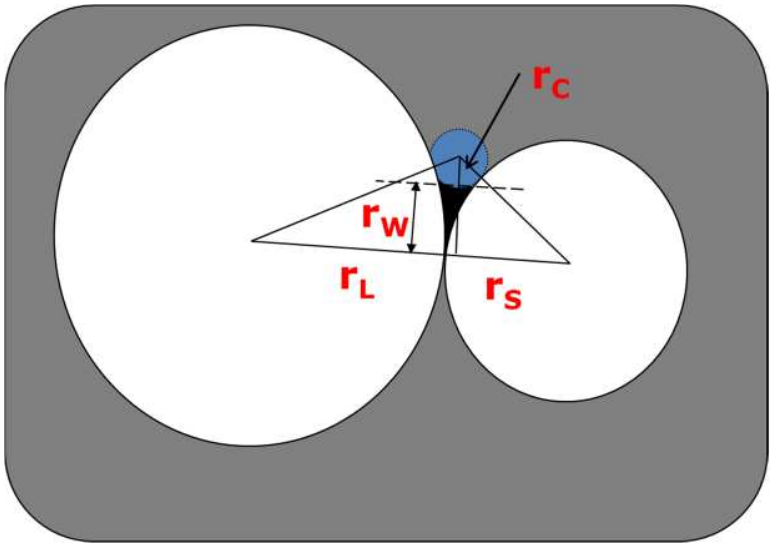

Fig 14 Simple geometric model to calculate the window radius, r_w , based on the bead radius and the capillary radius, r_c

Vitae

Andrew Kennedy is an Associate Professor within the Manufacturing Research Division at the University of Nottingham. He has expertise in light alloys and powder processing and his core research activity is in the field of multi-phase materials, with the main emphasis on processing-structure-property relationships in metal-ceramic composites and cellular and porous metals. He is a Fellow of the Institute of Materials, Minerals and Mining (IOM^3) and a Chartered Engineer, a consultant to UK industry on metal composites and foams and a UK technical expert adviser on metal foam testing standards.

Paul Langston is a lecturer in chemical engineering at the University of Nottingham, UK. He holds a PhD in Chemical Engineering from the University of Surrey. He has worked for many years both in academia and for consultants in mathematical modelling undertaking projects for commercial and defence organisations. His main areas of work are in computer simulation of particle and fluid flow, steady-state & dynamic process flow sheet simulations, crowd dynamics, monte-carlo models and applications of Bayes' theorem in engineering systems.